journal of materials processing technology 202 (2008) 464–474

journal homepage: www.elsevier.com/locate/jmatprotec

Artificial neural network modeling of weld joint strength prediction of a pulsed metal inert gas welding process using arc signals

Sukhomay Pal, Surjya K. Pal, Arun K. Samantaray*

Department of Mechanical Engineering, Indian Institute of Technology, Kharagpur 721302, India

ARTICLE INFO

Article history:
Received 11 April 2007
Received in revised form
13 September 2007
Accepted 26 September 2007

Keywords:
PMIGW
Weld strength monitoring
Artificial neural network
Response surface methodology
Multiple regression analysis

ABSTRACT

This paper addresses the weld joint strength monitoring in pulsed metal inert gas welding (PMIGW) process. Response surface methodology is applied to perform welding experiments. A multilayer neural network model has been developed to predict the ultimate tensile stress (UTS) of welded plates. Six process parameters, namely pulse voltage, back-ground voltage, pulse duration, pulse frequency, wire feed rate and the welding speed, and the two measurements, namely root mean square (RMS) values of welding current and voltage, are used as input variables of the model and the UTS of the welded plate is considered as the output variable. Furthermore, output obtained through multiple regression analysis is used to compare with the developed artificial neural network (ANN) model output. It was found that the welding strength predicted by the developed ANN model is better than that based on multiple regression analysis.

1. Introduction

The demand for online quality prediction has increased with the advancement of today's automated manufacturing environment. The total quality index of a product depends on the quality of output from every sub-process involved in the production chain and obviously, welding is one of the important sub-processes in most cases. As a result of this, there is a need for different technologies to precisely predict the weld quality with respect to the different welding operating conditions. There has been lots of research to predict the weld quality online; but a low cost, reliable, robust and industrially feasible monitoring system is not yet developed. Weld quality can be measured directly or indirectly. Direct methods are visual inspection and vision sensing (Sweet, 1985; Sforza and Blasiis, 2002) of the weld puddle. Indirect methods are arc sensing (Munezane et al., 1987; Cook et al., 1987; Hughes and Walduck, 1987; Cook, 1983), infrared sensing (Chin et al., 1983; Nagarajan et al., 1989; Chen and Chin, 1990), radiographic sensing (Rokhlin, 1989; Guu and Rokhlin, 1992), inductive sensing (Goldberg, 1985), sound sensing (Arata et al., 1981; Grad et al., 2004; Saini and Floyd, 1998), ultrasonic sensing (Bao and Ume, 2004; Carlson and Johnson, 1988) and acoustic emission sensing (Arata et al., 1981; Grad et al., 2004; Saini and Floyd, 1998). All the above-mentioned methods, which have been extensively used for online prediction of weld quality, use measurements of some signal(s) to correlate with the weld quality. Among the various sensors used, arc sensors, i.e., current and voltage sensors, are considered to be the most reliable, simple and competitive (Li et al., 2000; Siewert et al., 2002).

Arc sensors monitor the change in one or more of the electrical parameters of the arc, i.e., current and/or voltage. A

* *Corresponding author*. Tel.: +91 3222 282996; fax: +91 3222 255303.
E-mail address: skpal@mech.iitkgp.ernet.in (S.K. Pal).
0924-0136/$ – see front matter
doi:10.1016/j.jmatprotec.2007.09.039

large number of researchers (Munezane et al., 1987; Cook et al., 1987; Hughes and Walduck, 1987; Cook, 1983; Cook, 1981) have proposed arc sensing techniques for seam tracking in arc welding processes. In addition to this, arc sensing techniques are also used for online monitoring and control of the welding processes (Quinn et al., 1999). This technique can be used to detect arc start quality, steady state arc stability analysis, contact tip to workpiece distance variance, insufficient shielding gas coverage, electrode feeding problems, joint fit-up problems, electrode alignment errors, contact tip wear and metal transfer mode (Barborak et al., 1999).

Welding current and voltage signals are analyzed using power spectral density and time–frequency analysis method by Chu et al. (2004) for welding stability and weld quality monitoring in a short circuit gas metal arc welding (GMAW) process. Therein, by using time–frequency analysis method, the standard deviation and the mean of signals taken under normal operating conditions are compared to those of the signals under different abnormal operating conditions. Time domain analysis of voltage signal for monitoring welding quality in a short circuit GMAW process has been developed by Adolfsson et al. (1999). The repeated sequential probability ratio test was used therein to detect changes in weld quality, and variance of the welding voltage was used as a parameter of the algorithm. In (Johnson et al., 1991), a series of experiments have been performed by using two different power sources, namely transistor and transformer-rectifier power supply, and three different metal transfer modes. During the experiment, sound emission in audible range, welding current and welding voltage fluctuations were recorded. Those recorded signals were correlated to detect droplet transfer mode with the aid of the high-speed film data. High frequency and hybrid pulsed tungsten inert gas micro-welding process are monitored by Wang et al. (2003) through the arc sensing technique. The mean voltage of arc, probability density distribution of arc voltage, and the dynamic voltage–current graph of arc were used in that work to determine the weld penetration. The current and voltage signals are used by Rajasekaran et al. (1998) to determine the droplet detachment in a pulsed GMAW process. All the above mentioned monitoring systems work in a similar way, i.e., current, voltage and other process signals are measured, processed and then compared with some pre-set nominal values. An alarm is triggered when the deviation from the preset values exceeds a pre-chosen threshold. Use of static thresholds in process monitoring does not account for process uncertainties and it is generally less robust, i.e., there may be misdetections and false alarms. These discrepancies seriously jeopardize the efficiency of decision support systems and may lead to major losses, which could have been avoided with better fault isolation techniques.

Multilayer neural network is one of the simplest, robust and highly non-linear modeling techniques, and it is especially suitable for model-based supervision of uncertain systems. Moreover, this technique has been widely used for mapping input and output parameters of arc welding process. Andersen et al. (1990) pioneered the application of neural network in modeling an arc welding process. Since then, many researchers have modeled arc welding process by using various kinds of neural network models. Cook et al. (1995) used two back propagation network models for variable polarity plasma arc welding process modeling and control. For process modeling, they used a 4-10-2 network structure in which the input parameters were torch standoff distance, forward current, reverse current and torch travel speed, and the outputs were the weld crown width and the root width. For the process control or parameter selection, a network of a 2-10-4 structure was constructed to predict the torch standoff distance, forward current, reverse current and torch travel speed from the input given in the form of the desired crown width and root width. Their experimental work showed good agreement with the predicted outputs. In (Kang et al., 1999), an ANN model is developed to select welding parameters such as welding current, arc voltage, welding speed and weaving length for required output specifications given as weld bead shape, i.e., leg length, penetration, throat thickness and reinforcement height. An intelligent system for the automatic determination of optimal welding parameters for each pass and welding position is developed by Kim et al. (2006). A finite element model, two back propagation neural network models, and a corrective neural network model are used and validated therein. Predictions of the geometry of back-bead of MIG welding plates from an ANN model is compared with that of a multiple regression analysis model in Lee and Um (2000) and it was observed that the prediction error from the ANN model was smaller than that from the multiple regression analysis model. Fuzzy radial basis function neural network is used by Chi and Hsu (2001) for predicting weld quality characteristic of plasma arc welding. An ANN-based fuzzy logic control for fine tuning of the membership function and automatic fuzzy rules generation are developed by Di et al. (2001). Back propagation neural network model has also been used to predict the bead geometry and weld penetration in (Nagesh and Datta, 2002) where a 6-10-9-4 architecture was chosen as the optimal network structure by trial and error. A multilayer back propagation neural network for mapping input and output parameters has been used by Kim et al. (2004) where the pass number, welding speed, welding current and arc voltage are considered as input parameters, and bead width is the output parameter. Two specific training algorithms, the error-back propagation algorithm and Levenberg–Marquardt approximation algorithm were employed by Kim et al. (2004) to establish the network. Welded plate distortion has been predicted through an ANN model in Lightfoot et al. (2005) by considering the standard deviation as the measure of actual and predicted distortions, and it was found that the difference between the two data sets was significant.

However, few attempts have been made to correlate the arc signals to the weld quality using ANN. In the limited number of works reported in this direction, Ohshima et al. (1995) proposed a neuro-arc sensor model to simultaneously detect deviation, attitude and height of the torch. The welding current and voltage signals were used to train the neural network model, and then the trained model was used for monitoring of welding process and tracking of the weld line in a robotic MIG welding process. In another significant development, Quero et al. (1994) used current signal and ANN technique to monitor the weld quality. To increase the volume of information of the current waveforms, they divided the sampled current in eight energy levels by using histograms. Consequently, eight energy levels along with the shape factor of the current waveforms

Table 1 – Chemical composition of base metal (weight percentage)

C	0.139
Si	0.151
Mn	0.499
P	0.075
S	0.044
Ni	0.024
Cr	0.019
Cu	0.056

were used in a neural network to predict the failure load of the welded sample.

In this work, authors have developed an intelligent method for online prediction of the weld strength. The automatic calculation of the weld strength is evaluated by a pre-trained multilayer feed-forward neural network from signals taken during the welding process over moving measurement windows. The training and testing of the ANN model have been done using 53 experimental datasets, which were obtained from response surface analysis. The performance of the neural network is compared with the regression model, which has been developed from the same experimental datasets used for the neural network.

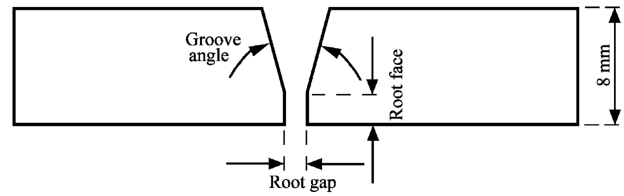

Fig. 1 – Profile of the edges of V-groove.

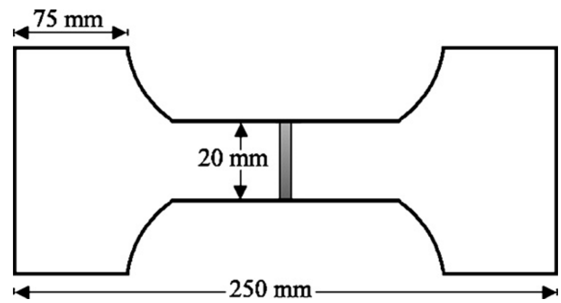

Fig. 2 – Tensile test specimen.

2. Experiments

2.1. Specimen preparation

In the present work, two mild steel specimens, with dimensions of 125 mm × 100 mm × 8 mm of each were used as the workpiece. Optical emission spectroscopy (OES) has been done to find out the chemical composition of the base metal, and is shown in Table 1. These specimens were prepared with V-shaped groove as shown in Fig. 1, where groove angle, root face and root gap were 30°, 2 mm and 2 mm, respectively. Thereafter, 53 pairs of such specimens with constant groove angle and root face were prepared, and then faces were cleaned by a surface grinder. To make a butt weld joint, two plates were tacked at the two ends along the width with constant root gap of 2 mm. Once the welding is over, all welded plates were cut to a required shape (Fig. 2.) to conduct the tensile test. Tensile tests were conducted at room temperature using a universal testing machine (make: Losenhausenwerk, Germany) on a 30 tonnes scale.

2.2. Equipment

A Fronius make welding machine is used in the present study. The power source is a constant voltage source, Transarc 500 and the control unit is VR131 type. A schematic diagram of the experimental setup is shown in Fig. 3. The welding torch or welding gun (model AW502) was mounted on a fixed arm (shown in Fig. 4). Mild steel plates were clamped on a motor-driven carriage with a variable speed in the range of 1 mm/s to 16 mm/s. Copper coated mild steel wire of 1.2 mm diameter is used in the experiment. This wire is fed through the welding gun by a four-roller drive system. Argon shielding gas was supplied at a flow rate of 15 l/min at a pressure of 10 kgf/cm^2.

A Hall-effect current transducer (LEM, model LT 500S) was fitted on the electrode to sense the welding current. Moreover,

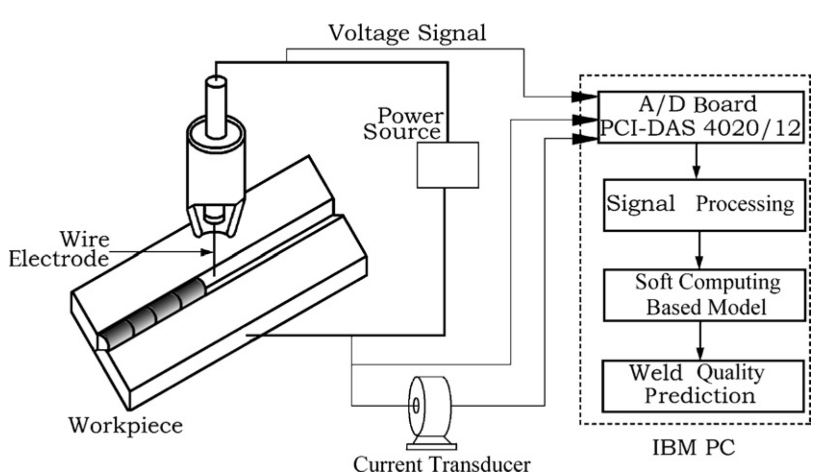

Fig. 3 – Schematic arrangement of the experimental setup.

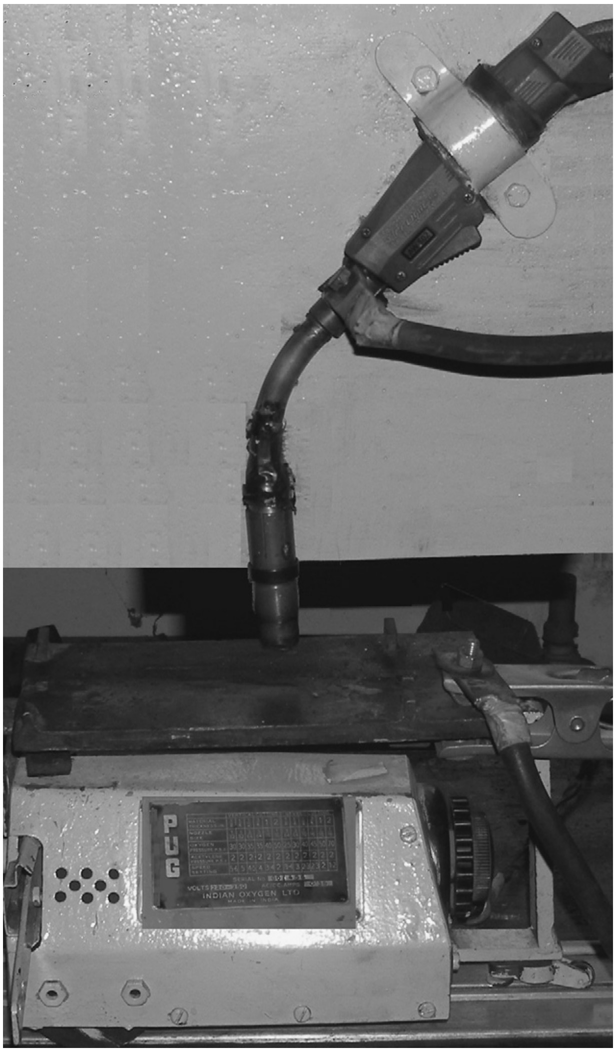

Fig. 4 – Welding gun with motor-driven table.

potential difference was sensed between the workpiece and the contact tip. The measured voltage was stepped down in 1:11 ratio before feeding to the A/D card (make Measurement Computing Corporation, model: PCI-DAS 4020/12). The analog outputs from these sensors were converted into digital signals by an A/D card fitted to an IBM PC. The signals were sampled at 10 kHz, and the magnitude of the sensor output was measured in ±5 V range.

2.3. *Experimental procedure*

The objective of this experiment is to determine and represent the cause and effect relationship between the response and input control variables. Taguchi method is useful in this regard to understand the influence that parameters had on variation, not just on the mean (Datta et al., in press). In conventional design of experiments, variation between experimental replications is a nuisance that the experimenter would like to eliminate whereas, in Taguchi's method, it is a central object of investigation. Taguchi method relies on the replication each experiment by means of an outer array, itself an orthogonal array that seeks deliberately to emulate the sources of variation that a product would encounter in reality. On the other hand, response surface methodology (RSM) explores the relationships between several explanatory variables and one or more response variables. The main idea of RSM is to use a set of designed experiments to obtain an optimal response. Although this model is only an approximation, it is easy to estimate and apply, even when little is known about the process. Due to the very complicated nature of the welding process, which involves electrical, thermal, hydraulic, plasma-physics and thermo-metallurgical phenomena, and more importantly, unavailability of sufficient knowledge about the process dynamics, RSM methodology was preferred in this paper over Taguchi method.

A three level, six factors, half fraction central composite experimental design with nine center points was performed which requires 53 experimental runs. A commercially available software package, MINITAB (Minitab Inc., 2000), was used to setup the design matrix. The design matrix is shown in Table 2.

3. Modeling of the PMIG welding process

In this work, two different modeling techniques such as artificial neural network, and a multiple regression analysis have been done.

3.1. *Artificial neural network modeling*

Artificial neural networks have proved useful in a variety of real-world application that deal with complex and highly interactive processes, like pattern recognition, speech recognition, finance, medicine, sales forecasting, weather forecasting, and monitoring and control of a manufacturing processes. The advantage of this approach is that modeling can be done using experimental data without having to make any simplifying assumption. Various types of ANN, like multilayer perception (MLP), radial basis function (RBF), self-organizing map (SOM), etc. are used for modeling. However, MLP, which is generally trained with the back propagation error algorithm, is popularly used in the weld modeling (Kim et al., 2006; Lee and Um, 2000; Chi and Hsu, 2001; Lightfoot et al., 2005; Ohshima et al., 1995). In this research, a code for multi-neuron, multi-hidden layer ANN model has been developed in C programming language, for mapping the pulsed metal inert gas welding (PMIGW) process parameters such as pulse voltage, back-ground voltage, pulse duration, pulse frequency, wire feed-rate, welding speed and RMS values of current and voltage signals to the ultimate tensile stress of the resulting weld joint. A schematic representation of a fully connected multi-neuron, multi-hidden layer ANN architecture is shown in Fig. 5, which was employed in this research. The network consists of an input layer, varying number of hidden layers and an output layer. All nodes of a layer are connected to all the nodes of the adjacent layers, and the numbers of hidden layers and the number of neurons in different hidden layers have been varied. The input layer receives the information from an external source, which is subsequently multiplied by the interconnection weights between it and the adjacent hidden layer and then the products are summed up. The summation of products is modified

Table 2 – Design matrix of experimental run with response

Experiment no.	Back-ground voltage (V)	Pulse voltage (V)	Pulse frequency (Hz)	Pulse duty factor	Wire feed rate (m/min)	Table feed rate (mm/s)	RMS current (V)	RMS voltage (V)	UTS (MPa)
1	17	34.6	130	0.5	9	3.76	1.1939	2.7429	412.28
2	17	34.6	130	0.5	9	3.76	1.1415	2.7449	415.79
3	14	30	80	0.35	11	5.635	1.4385	1.6834	0
4	14	39	80	0.35	7	5.635	1.1971	2.7190	328.71
5	14	30	182	0.65	11	5.635	1.2566	2.3814	385.98
6	20	39	80	0.65	7	5.635	1.2773	3.2596	246.92
7	14	39	80	0.65	7	2.456	1.2791	3.1528	353.40
8	17	34.6	130	0.50	7	3.76	1.0516	2.7334	329.75
9	20	30	80	0.35	11	2.456	1.4692	1.9772	0
10	17	34.6	130	0.5	9	5.635	1.1839	2.6688	214.38
11	17	34.6	182	0.5	9	3.76	1.1434	2.6927	452.31
12	17	30	130	0.5	9	3.76	1.1998	2.3022	190.69
13	14	30	80	0.65	7	5.635	0.9921	2.4823	193.88
14	20	39	80	0.35	7	2.456	1.1052	2.9427	463.03
15	20	30	182	0.65	11	2.456	1.4019	2.3886	231.11
16	17	34.6	130	0.5	9	3.76	1.1493	2.7500	412.53
17	17	34.6	130	0.5	9	3.76	1.1945	2.7313	419.28
18	14	30	182	0.35	11	2.456	1.5672	1.7755	0
19	14	39	80	0.65	11	5.635	1.5484	2.9822	461.73
20	14	30	80	0.65	11	2.456	0.7498	2.6086	331.28
21	17	34.6	130	0.5	9	3.76	1.1650	2.7508	411.85
22	17	34.6	130	0.65	9	3.76	1.2652	2.8668	419.00
23	20	30	182	0.35	7	2.456	1.0122	2.4273	371.65
24	17	34.6	130	0.5	9	3.76	1.1989	2.7081	417.33
25	20	39	182	0.35	11	2.456	1.3841	2.6365	375.44
26	17	34.6	80	0.5	9	3.76	1.1516	2.7705	403.06
27	20	30	182	0.35	11	5.635	1.3825	1.9676	0
28	14	34.6	130	0.5	9	3.76	1.1673	2.6496	424.97
29	17	34.6	130	0.5	9	2.456	1.1965	2.7268	463.80
30	14	39	182	0.35	11	5.635	1.3096	2.4468	282.97
31	20	39	182	0.65	7	2.456	1.246	3.2878	263.60
32	20	30	182	0.65	7	5.635	1.0026	2.5803	370.21
33	20	30	80	0.65	11	5.635	1.2856	2.4107	251.88
34	17	34.6	130	0.35	9	3.76	1.2128	2.3691	293.29
35	14	39	182	0.65	11	2.456	1.3787	3.1774	418.95
36	14	39	182	0.65	7	5.635	1.2979	3.1505	232.75
37	20	39	182	0.65	11	5.635	1.2026	2.7367	455.13
38	17	34.6	130	0.50	9	3.76	1.1717	2.7386	420.97
39	14	30	182	0.35	7	5.635	1.0123	2.0132	11.523
40	20	30	80	0.35	7	5.635	0.9973	2.2885	189.19
41	17	39	130	0.5	9	3.76	1.3221	2.9732	443.87
42	20	30	80	0.65	7	2.456	0.9922	2.6553	436.47
43	14	30	80	0.35	7	2.456	1.0072	2.2308	15.20
44	14	39	80	0.35	11	2.456	1.4916	2.2187	109.34
45	14	30	182	0.65	7	2.456	0.9790	2.6119	356.67
46	17	34.6	130	0.5	11	3.76	1.3023	2.5549	402.58
47	20	39	182	0.35	7	5.635	1.1497	2.5602	265.93
48	17	34.6	130	0.5	9	3.76	1.2161	2.7163	410.64
49	20	39	80	0.65	11	2.456	1.3634	3.2698	453.11
50	20	39	80	0.35	11	5.635	1.3265	2.7507	367.01
51	14	39	182	0.35	7	2.456	1.1070	2.6931	445.03
52	17	34.6	130	0.5	9	3.76	1.1947	2.6984	413.43
53	20	34.6	130	0.5	9	3.76	1.1786	2.6165	349.20

by an activation function (in this case, sigmoid, a transfer function) and these modified values in turn become the output signal for the first hidden layer and input signal for the next layer. In this way, the signal finally reaches to the output layer, where it is terminated at the external receptor node(s). The network was trained in a supervised manner with error-back propagation algorithm.

3.2. *Regression modeling*

In this work, relation between the PMIGW process parameters, namely pulse voltage (V_P), back-ground voltage (V_B), pulse duration (T_P), pulse frequency (f), wire feed rate (F_{wire}), welding speed (F_{weld}) and RMS values of welding current ($RMS_{current}$) and voltage ($RMS_{voltage}$), and the process output

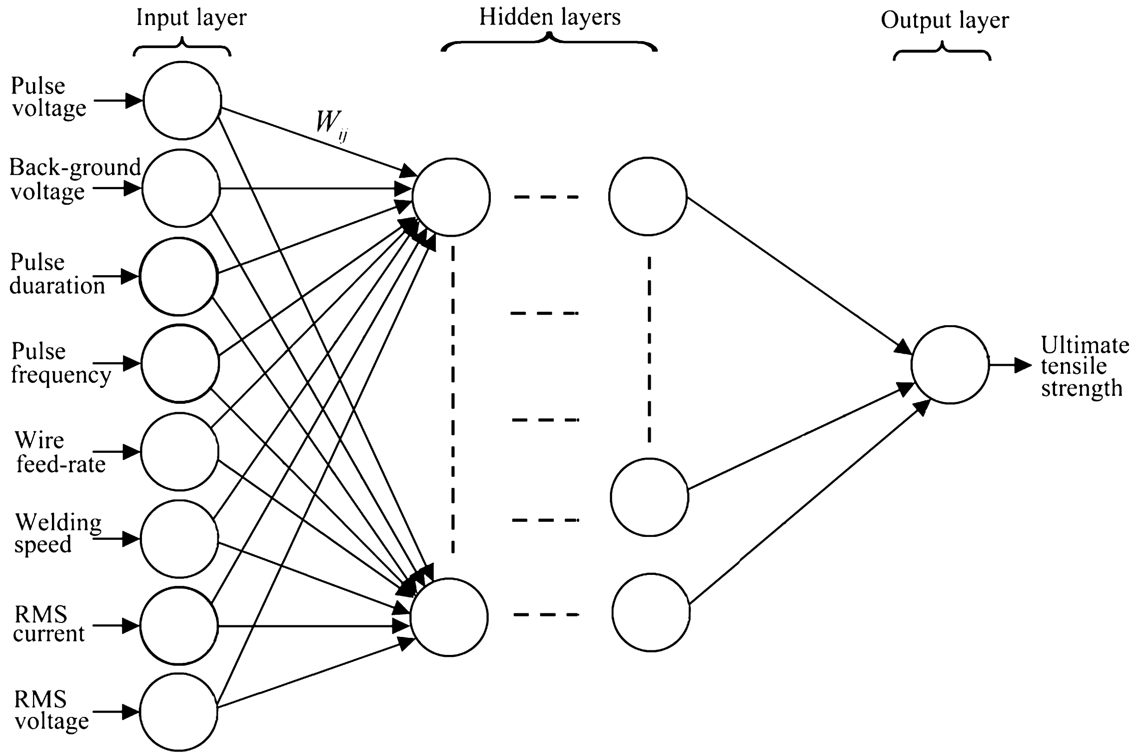

Fig. 5 – A schematic diagram of multilayer neural network.

specified as ultimate tensile stress (S) was examined. Three regression models are developed: (1) first degree liner model, (2) second degree surface model, and (3) power model. The expressions of these three models are shown in Eqs. (1)–(3), respectively.

$$S = c_0 + c_1 V_B + c_2 V_P + c_3 f + c_4 T_P + c_5 F_{wire} + c_6 F_{weld} + c_7\,\mathrm{RMS}_{current} + c_8\,\mathrm{RMS}_{voltage}, \quad (1)$$

where c_i ($i = 0, \ldots, 8$) are constants.

$$\begin{aligned} S = {} & a_0 + a_1 V_B + a_2 V_P + a_3 f + a_4 T_P + a_5 F_{wire} + a_6 F_{weld} + a_7\,\mathrm{RMS}_{current} + a_8\,\mathrm{RMS}_{voltage} + a_{12} V_B V_P \\ & + a_{13} V_B f + a_{14} V_B T_P + a_{15} V_B F_{wire} + a_{16} V_B F_{weld} + a_{17} V_B\,\mathrm{RMS}_{current} + a_{18} V_B\,\mathrm{RMS}_{voltage} + a_{23} V_P f \\ & + a_{24} V_P T_P + a_{25} V_P F_{wire} + a_{26} F_{weld} V_P + a_{27} V_P\,\mathrm{RMS}_{current} + a_{28} V_P\,\mathrm{RMS}_{voltage} + a_{34} f T_P + a_{35} f F_{wire} \\ & + a_{36} f F_{weld} + a_{37} f\,\mathrm{RMS}_{current} + a_{38} f\,\mathrm{RMS}_{voltage} + a_{45} T_P F_{wire} + a_{46} T_P F_{weld} + a_{47} T_P\,\mathrm{RMS}_{current} \\ & + a_{48} T_P\,\mathrm{RMS}_{voltage} + a_{56} F_{wire} F_{weld} + a_{57} F_{wire}\,\mathrm{RMS}_{current} + a_{58} F_{wire}\,\mathrm{RMS}_{voltage} \\ & + a_{67} F_{weld}\,\mathrm{RMS}_{current} + a_{68} F_{weld}\,\mathrm{RMS}_{voltage} + a_{78}\,\mathrm{RMS}_{current}\,\mathrm{RMS}_{voltage} \end{aligned} \quad (2)$$

where a_i ($i = 0, \ldots, 8$), a_{ij} ($i = 1, \ldots, 7$, $j = i+1, \ldots, 7$) are constants.

$$S = b_0 V_B^{b_1} V_P^{b_2} f^{b_3} T_P^{b_4} F_{wire}^{b_5} F_{weld}^{b_6}\,\mathrm{RMS}_{current}^{b_7}\,\mathrm{RMS}_{voltage}^{b_8} \quad (3)$$

where b_i ($i = 0, \ldots, 8$) are constants.

The coefficients of these regression equations are obtained by applying least square error minimization of the experimental data.

4. Experimental results

The experiments were conducted as per the design matrix given in Table 2 wherein the response values of ultimate tensile stress (UTS) of the welded plates and the calculated values of RMS of current and voltage signals are also given.

Some of the welded plates, which broke during the sample preparation to conduct the tensile test, are considered to have zero UTS. Two examples of recorded actual welding current and voltage signals corresponding to the experimentally obtained maximum and minimum UTS are shown in Figs. 6 and 8, respectively, and their magnified views over shorter time span are given in Figs. 7 and 9, respectively.

5. Prediction of weld strength

From the arc signal analysis, as shown in Figs. 6–9, it is well understood that the welding current and voltage can be used to detect weld strength. Therefore, in the present work, a back propagation neural network model was trained on randomly

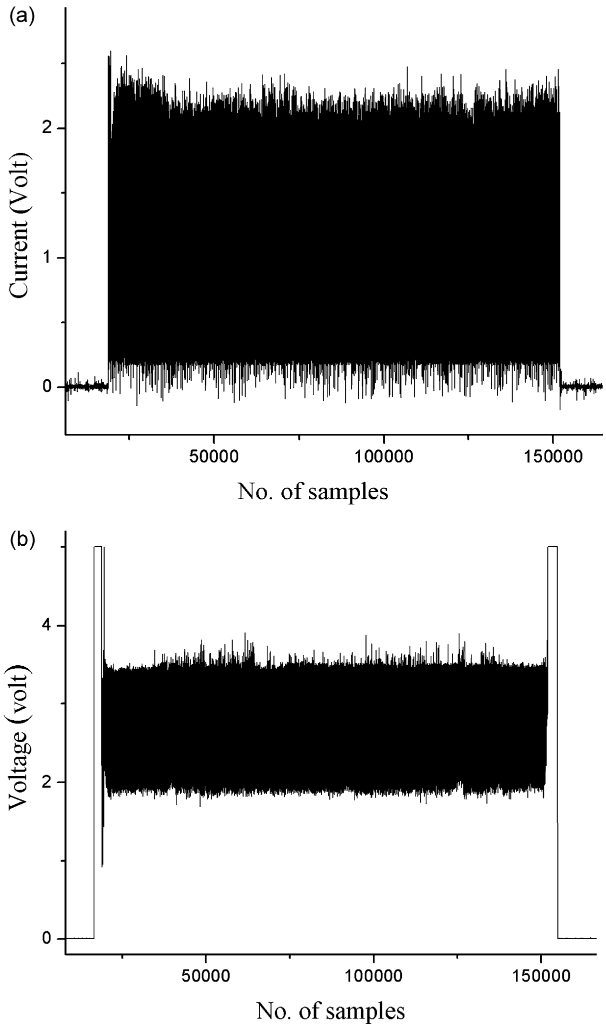

Fig. 6 – Arc signal at maximum weld strength: (a) current signal and (b) voltage signal.

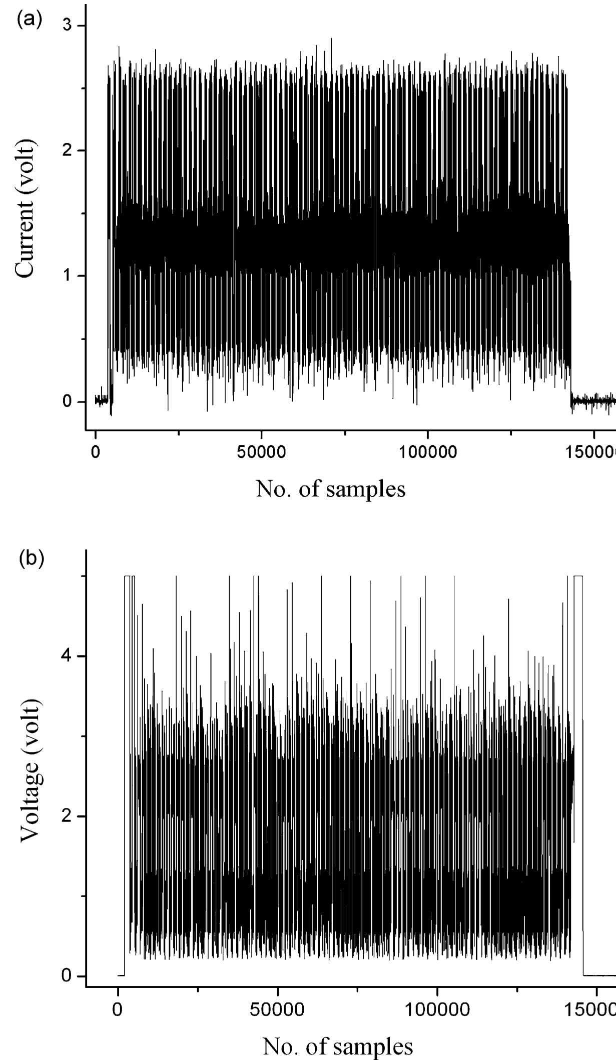

Fig. 8 – Arc signal at minimum weld strength: (a) current signal and (b) voltage signal.

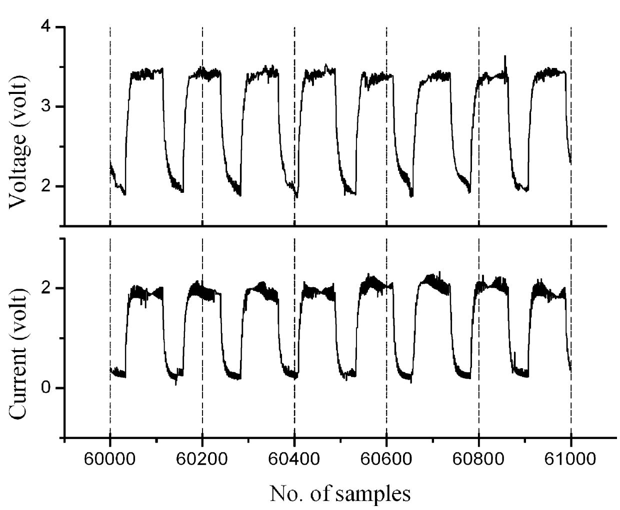

Fig. 7 – Magnified views of the signals in Fig. 6(a) and (b).

selected dataset of 46 input–output pairs in a batch mode. Initial weight values were chosen randomly between ±0.9, and the bias value at the input layer was taken as zero and those of hidden and output layers as one. All the input and output variables were normalized between 0.1 and 0.9. The training objective was mean square error (MSE) minimization by updating the weights through the gradient descent method.

$$\mathrm{MSE} = \frac{1}{N}\sum_{i}^{N}(T_i - O_i^k)^2 \quad (4)$$

where N is the total number of training dataset, T_i is the target output of ith dataset, i.e., experimental output of ith dataset, and O_i^k is the output from the ANN model on kth iteration when ith dataset is considered the network input. The performance of a neural network depends on number of hidden layers, number of neurons in the hidden layers, learning rate and momentum coefficient. Therefore, several combinations should be tried out to choose an optimal combination. In this work, single and double hidden layer(s) were tried. In

Table 3 – Performance of different ANN architectures with different learning rates and momentum coefficients

Serial no.	ANN structure	Learning rate	Momentum coefficient	MSE training $\times 10^3$	MSE testing $\times 10^2$
1	8-6-1	0.9	0.5	0.980	6.227
2	8-7-1	0.9	0.5	0.668	0.974
3	8-8-1	0.9	0.5	0.205	0.496
4	8-9-1	0.9	0.5	0.057	2.198
5	8-10-1	0.9	0.5	0.075	2.289
6	8-11-1	0.9	0.5	0.249	1.567
7	8-12-1	0.9	0.5	0.828	0.813
8	8-13-1	0.9	0.5	0.663	0.814
9	8-14-1	0.9	0.5	0.149	2.341
10	8-15-1	0.9	0.5	0.324	3.237
11	8-16-1	0.9	0.5	0.052	1.274
12	8-17-1	0.9	0.5	0.416	3.163
13	8-18-1	0.9	0.5	0.167	1.075
14	8-19-1	0.9	0.5	0.147	1.989
15	8-20-1	0.9	0.5	0.052	0.488
16	8-21-1	0.9	0.5	0.163	2.099
17	8-22-1	0.9	0.5	0.101	0.942
18	8-23-1	0.9	0.5	0.124	0.931
19	8-24-1	0.9	0.5	0.635	2.073
20	8-25-1	0.9	0.5	0.092	2.452
21	8-8-8-1	0.9	0.5	0.403	1.556
22	8-8-10-1	0.9	0.5	0.799	0.279
23	8-8-12-1	0.9	0.5	0.645	1.701
24	8-8-14-1	0.9	0.5	0.246	0.226
25	8-8-16-1	0.9	0.5	0.789	3.399
26	8-8-18-1	0.9	0.5	0.847	0.767
27	8-8-20-1	0.9	0.5	1.404	1.394
28	8-8-22-1	0.9	0.5	1.217	1.389
29	8-12-6-1	0.9	0.5	0.543	2.524
30	8-12-8-1	0.9	0.5	0.479	1.494
31	8-12-10-1	0.9	0.5	0.379	0.571
32	8-12-12-1	0.9	0.5	0.067	0.714
33	8-12-14-1	0.9	0.5	0.283	0.831
34	8-12-16-1	0.9	0.5	0.527	0.806
35	8-12-18-1	0.9	0.5	0.562	0.906
36	8-12-20-1	0.9	0.5	0.513	0.460
37	8-12-22-1	0.9	0.5	0.543	2.167
38	8-13-6-1	0.9	0.5	1.250	1.870
39	8-13-8-1	0.9	0.5	0.874	1.076
40	8-13-10-1	0.9	0.5	0.566	0.204
41	8-13-12-1	0.9	0.5	0.436	0.214
42	8-13-14-1	0.9	0.5	0.461	2.711
43	8-13-16-1	0.9	0.5	1.654	1.599
44	8-13-18-1	0.9	0.5	0.514	0.104
45	8-13-20-1	0.9	0.5	0.373	0.671
46	8-13-22-1	0.9	0.5	0.579	2.538
47	8-20-6-1	0.9	0.5	63.041	2.994
48	8-20-8-1	0.9	0.5	0.963	2.228
49	8-20-10-1	0.9	0.5	2.822	1.285
50	8-20-12-1	0.9	0.5	1.337	0.261
51	8-20-14-1	0.9	0.5	1.382	0.239
52	8-13-18-1	0.9	0.55	0.486	0.116
53	8-13-18-1	0.9	0.6	0.523	0.116
54	8-13-18-1	0.9	0.65	0.565	0.114
55	8-13-18-1	0.9	0.7	0.616	0.114
56	8-13-18-1	0.9	0.75	0.656	0.117
57	8-13-18-1	0.9	0.45	0.595	0.114
58	8-13-18-1	0.9	0.4	0.542	0.103
59	**8-13-18-1**	**0.9**	**0.35**	**0.466**	**0.098**
60	8-13-18-1	0.9	0.3	0.411	0.115
61	8-13-18-1	0.95	0.35	0.394	0.128
62	8-13-18-1	0.85	0.35	0.596	0.114
63	8-13-18-1	0.8	0.35	0.487	0.110
64	8-13-18-1	0.75	0.35	0.530	0.114
65	8-13-18-1	0.7	0.35	0.617	0.110
66	8-13-18-1	0.65	0.35	0.666	0.114

Bold values correspond to best network model.

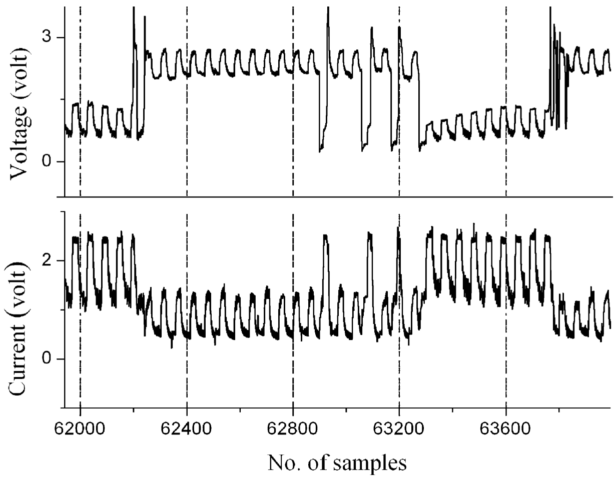

Fig. 9 – Magnified views of the signals in Fig. 8 (a) and (b).

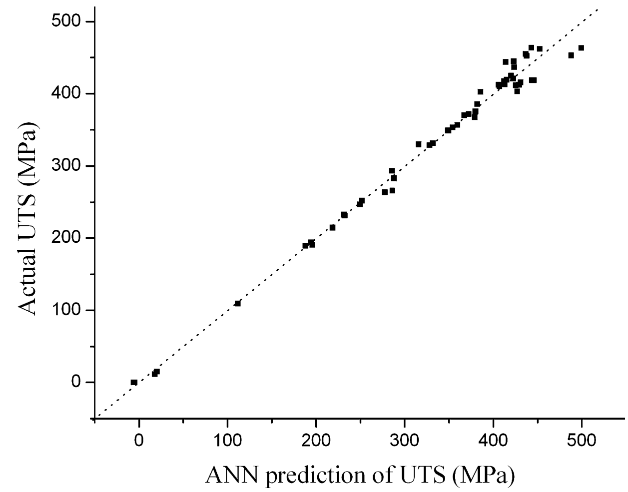

Fig. 10 – Scatter diagram of ANN prediction vs. actual UTS.

the single hidden layer structure, the number of neurons in the hidden layer was varied from 6 to 25 and in double hidden layers structure; the numbers of neurons in the first hidden layer was varied from 8 to 20, and for the second hidden layer from 6 to 22. Learning rate and momentum coefficient were varied between 0.65–0.95 and 0.3–0.75, respectively, in both of the above cases. After training the network, seven remaining datasets were used to test the network performance. The performance of different ANN architectures with different learning rate and momentum coefficient are shown in Table 3. The scatter diagram of training and testing datasets is shown in Fig. 10, based on the prediction of the best architecture (8-13-18-1). The ANN predicted values and percentage errors in the output (UTS) are shown in Table 4.

In addition to ANN model, the weld strength is predicted using regression analysis. The regression equations given in Eqs. (1)–(3) are solved using the least square method (Gunaraj and Murugan, 1999; Takeshita, 2000). The same datasets, as used in ANN model, were used to develop and evaluate the performance of the model. After evaluation of the coefficients in the regression equations, they are inserted in Eqs. (1)–(3), and the final form of the static regression model equations are given in Eqs. (5)–(7), respectively.

$$S = -526 + 2.09V_B - 7V_P + 0.238f - 2.51T_P + 44.4F_{wire} - 2F_{weld} - 328\,RMS_{current} + 438\,RMS_{voltage} \quad (5)$$

$$\begin{aligned}S = {} & -12054 + 215.7V_B + 447.5V_P - 0.06f + 51.9T_P - 30.1F_{wire} + 86.2F_{weld} + 2650\,RMS_{current} - 248\,RMS_{voltage} \\ & -19.11V_BV_P + 0.083V_Bf - 2.83V_BT_P + 7.43V_BF_{wire} - 2.318V_BF_{weld} - 59.5V_B\,RMS_{current} + 225.6V_B\,RMS_{voltage} \\ & +1.2365V_Pf + 2.297V_PT_P - 16.63V_PF_{wire} - 3.22F_{weld}V_P - 24.5V_P\,RMS_{current} - 79.09V_P\,RMS_{voltage} + 0.256fT_P \\ & +0.538fF_{wire} - 0.753fF_{weld} - 14.045f\,RMS_{current} - 15.606f\,RMS_{voltage} + 0.17T_PF_{wire} + 2.826T_PF_{weld} \\ & -62.18T_P\,RMS_{current} - 19.14T_P\,RMS_{voltage} - 19.79F_{wire}F_{weld} + 27.2F_{wire}\,RMS_{current} + 165.9F_{wire}\,RMS_{voltage} \\ & +387F_{weld}\,RMS_{current} - 124.6F_{weld}\,RMS_{voltage} + 1012\,RMS_{current}\,RMS_{voltage}\end{aligned} \quad (6)$$

$$S = 6.3096 \times 10^{-6} V_B^{-2.3} V_P^{-2.47} f^{0.858} T_P^{2.29} F_{wire}^{4.275} F_{weld}^{1.167} RMS_{current}^{-13.364} RMS_{voltage}^{29.23} \quad (7)$$

The values of the regression coefficient (R^2) for the first degree liner equation, second degree surface equation and power equation are found to be 0.664, 0.971 and 0.688, respectively. Among these three models, R^2 value of second degree surface equation is near to unity. Therefore, this model is

Table 4 – Actual values, ANN and regression model predicted values of testing dataset with percentage error

Sl. no.	Actual UTS	ANN model predicted UTS	Percentage error in ANN prediction	Regression model predicted UTS	Percentage error in regression model prediction
1	265.93	286.50	−7.735	69.752	73.770
2	410.64	407.20	0.836	421.731	−2.701
3	453.11	488.19	−7.741	500.179	−10.387
4	367.01	379.53	−3.411	28.293	92.291
5	445.03	423.24	4.898	630.347	−41.641
6	413.43	412.87	0.133	413.445	−0.005
7	349.20	349.34	−0.040	408.643	−17.022
Mean absolute percentage errors			3.542		33.974

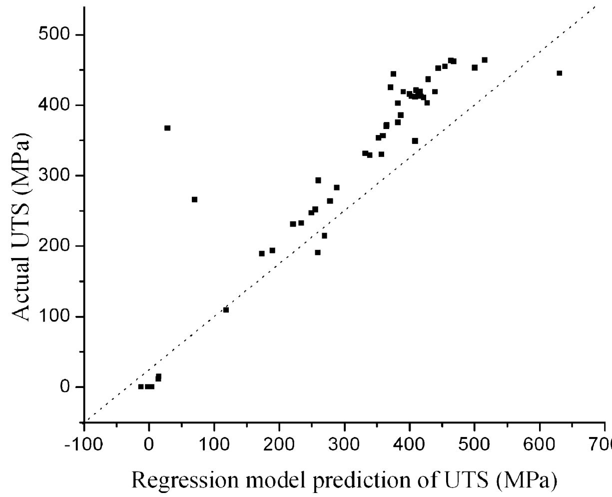

Fig. 11 – Scatter diagram of regression model (Eq. (6)) prediction vs. actual UTS.

considered best for representing input–output relationship of PMIGW process. The response calculated from this model for all datasets is shown in Fig. 11 and the prediction values and percentage errors in UTS are shown in Table 4 along with the results from the ANN model.

Results of the ANN and multiple regression analysis (Eq. (6)) were compared by using seven test datasets, in terms of percentage error. The following observations can be made from the results, as shown in Table 4.

(1) The architecture 8-13-18-1 with learning rate of 0.9 and momentum coefficient of 0.35 gives the lowest prediction error.
(2) The prediction obtained from the neural network model is within ±8% of the actual values and therefore, this model may be used for online prediction of weld strength with sufficient accuracy.

6. Conclusion

This work focuses on the ultimate tensile stress prediction in PMIGW process from statistical properties of measured arc signals and process parameters by using an ANN model. A series of experiments were carried out by applying response surface method, which evenly distributes the process parameters over the operating range. Then obtained experimental data was used to train and test ANN model of various architectures; and 8-13-18-1 architecture with learning rate and momentum coefficient of 0.9 and 0.35, respectively, was found as the best one for the current purpose. A multiple regression model was also developed and its performance was compared with the performance of the ANN model. It was found that the error in prediction of weld strength from the neural network model is less than that from the regression model. Therefore, the developed technique, which is based on an ANN model having process parameters and monitored arc signal properties as inputs, may be used for online prediction of weld strength in PMIGW processes.

REFERENCES

Adolfsson, S., Bahrami, A., Bolmsjo, G., Claesson, I., 1999. On-line quality monitoring in short-circuit gas metal arc welding. Weld. J. 78, 59–73.

Andersen, K., Cook, G.E., Karsai, G., Ramaswamy, K., 1990. Artificial neural networks applied to arc welding process modeling and control. IEEE Trans. Ind. Appl. 26, 824–830.

Arata, Y., Inoue, K., Futamata, M., Toh, T., 1981. Investigation on welding arc sound: vibration analysis of base metal during welding. Trans. JWRI 10, 39–45.

Bao, M., Ume, I.C., 2004. Three-dimensional ray tracing of laser ultrasound for weld penetration sensing. J. Acoust. Soc. Am. 115, 1565–1571.

Barborak, D., Conrardy, C., Madigan, B., Paskell, T., 1999. Through-arc process monitoring techniques for control of automated gas metal arc welding. In: Proceedings of the International Conference on Robotic and Automation, vol. 4, IEEE, Detroit, MI, pp. 3053–3058.

Carlson, N.M., Johnson, J.A., 1988. Ultrasonic sensing of weld pool penetration. Weld. J. 67, 239–246.

Chen, W.H., Chin, B.A., 1990. Monitoring weld penetration using infrared sensing techniques. Weld. J. 69, 181–185.

Chi, S.C., Hsu, L.C., 2001. A fuzzy radial basis function neural network for predicting multiple quality characteristics of plasma arc welding. In: IFSA World Congress & 20th NAFIPS International Conference, vol. 5, Vancouver, Canada, pp. 2807–2812.

Chin, B.A., Madsen, N.H., Goodling, J.S., 1983. Infrared thermography for sensing the arc welding process. Weld. J. 62, 227–234.

Chu, Y.X., Hu, S.J., Hou, W.K., Wang, P.C., Marin, S.P., 2004. Signature analysis for quality monitoring in short circuit GMAW. Weld. J. 83, 336–343.

Cook, G.E., 1981. Feedback and adaptive control in automated arc welding systems. Met. Construction 13, 551–556.

Cook, G.E., 1983. Through the arc sensing of arc welding. In: Proceedings Conference Production Research Technology. SAE Publication, pp. 141–151.

Cook, G.E., Andersen, K., Fernandez, K.R., Shepard, M.E., Wells, A.M., 1987. Electric arc sensing for robot positioning control. In: Lane, J.D. (Ed.), Robotic Welding. IFS Publications Ltd., London, pp. 182–216.

Cook, G.E., Barnett, R.J., Andersen, K., Strauss, A.M., 1995. Weld modeling and control using artificial neural networks. IEEE Trans. Ind. Appl. 31, 1484–1491.

Datta, S., Bandyopadhyay, A., Pal, P.K., in press. Modeling and optimization of features of bead geometry including percentage dilution in submerged arc welding using mixture of flux and fused slag, J. Adv. Manuf. Technol., doi:10.1007/s00170-006-0894-7.

Di, L., Srikanthan, T., Chandel, R.S., Katsunori, I., 2001. Neural-network based self-organized fuzzy logic control for arc welding. Eng. Appl. Artif. Intell. 14, 115–124.

Goldberg, F., 1985. Inductive seam-tracking improves mechanized and robotic welding. In: Proceedings of International Conference on Automation and Robotisation in Welding and Allied Processes. International Institute of Welding, France, pp. 393–400.

Grad, L., Grum, J., Polajnar, I., Slabe, J.M., 2004. Feasibility study of acoustic signals for on-line monitoring in short circuit gas metal arc welding. Int. J. Mach. Tools Manuf. 44, 555–561.

Gunaraj, V., Murugan, N., 1999. Application of response surface methodology for predicting weld bead quality in submerged arc welding of pipes. J. Mater. Process. Technol. 88, 266–275.

Guu, A., Rokhlin, S., 1992. Arc weld process control using radiographic sensing. Mater. Eval. 50, 1344–1348.

Hughes, R.V., Walduck, R.P., 1987. Electromagnetic arc path control I plasma welding. In: Lane, J.D. (Ed.), Robotic Welding. IFS Publications Ltd., London, pp. 2244–2263.

Johnson, J.A., Carlson, N.M., Smartt, H.B., Clark, D.E., 1991. Process control of GMAW: sensing of metal transfer mode. Weld. J. 70, 91–99.

Kang, S.I., Kim, G.H., Lee, S.B., 1999. A study on the horizontal fillet welding using neural networks. In: Proceedings of the third International Conference on Knowledge-based Intelligent Information Engineering Systems, IEEE, Australia, pp. 217–221.

Kim, I.S., Son, J.S., Lee, S.H., Yarlagadda, P.K.D.V., 2004. Optimal design of neural networks for control in robotics arc welding. Rob. Comput.-Integr. Manuf. 20, 57–63.

Kim, I.S., Jeong, Y.J., Lee, C.W., Yarlagadde, P.K.D.V., 2006. Prediction of welding parameters for pipeline welding using an intelligent system. J. Adv. Manuf. Technol. 22, 713–719.

Lee, J., Um, K., 2000. A comparison in a back-bead predication of gas metal arc welding using multiple regression analysis and artificial neural networks. Opt. Laser Eng. 34, 149–158.

Li, D., Yonglun, S., Feng, Y., 2000. On line monitoring of weld defects for short-circuit gas metal arc welding based on the self-organize feature map neural networks. Proc. Int. Joint Conf. Neural Netw. 5, 239–244.

Lightfoot, M.P., Bruce, G.J., McPherson, N.A., Woods, K., 2005. The application of artificial neural networks to weld-induced deformation in ship plate. Weld. J. 84, 23–30.

Minitab Inc., 2000. User Manual of MINITAB™ Statistical Software, Release 13.31. Minitab Inc., State College, PA, USA, 2000.

Munezane, Y., Watanabe, T., Iochi, A., Sekino, T., 1987. A sensing system for arc welding. In: Lane, J.D. (Ed.), Robotic Welding. IFS Publications Ltd., London, pp. 265–274.

Nagarajan, S., Chen, W.H., Chin, B.A., 1989. Infrared sensing for adaptive arc welding. Weld. J. 68, 462–466.

Nagesh, D.S., Datta, G.L., 2002. Prediction of weld bead geometry and penetration in shielded metal-arc welding using artificial neural networks. J. Mater. Process. Technol. 123, 303–312.

Ohshima, K., Yabe, M., Akita, K., Kugai, K., Kubota, T., Yamane, S., 1995. Sensor fusion using neural network in robotic welding. Ind. Appl. Conf. IEEE 2, 1764–1769.

Quero, J.M., Millan, R.L., Franquelo, L.G., 1994. Neural network approach to weld quality monitoring. In: Proceedings of 20th International Conference on Industrial Electronics, Control and Instrumentation, IEEE, vol. 2, pp. 1287–1291.

Quinn, T.P., Smith, C., Mccowan, C.N., Blachowiak, E., Madigan, R.B., 1999. Arc sensing for defects in constant voltage gas metal arc welding. Weld. J. 79, 322–328.

Rajasekaran, S., Kulkarni, S.D., Mallya, U.D., Chaturvedi, R.C., 1998. Droplet detachment and plate fusion characteristics in pulsed current gas metal arc welding. Weld. J. 78, 254–269.

Rokhlin, S., 1989. In-process radiographic evaluation of arc welding. Mater. Eval. 47, 219–224.

Saini, D., Floyd, S., 1998. An investigation of gas metal arc welding sound signature for on-line quality control. Weld. J. 77, 172–179.

Sforza, P., Blasiis, D.D., 2002. On-line optical monitoring system for arc welding. NDT&E Int. 35, 37–43.

Siewert, T., Samardzic, I., Klaric, S., 2002. Application of an on-line weld monitoring system. In: Proceedings of the first International Conference on Advanced Technologies for Developing Countries, Slavonski Brod, Croatia.

Sweet, L.M., 1985. Sensor-based control systems for arc welding robots. Rob. Comp.-Integr. Manuf. 2, 125–133.

Takeshita, K., 2000. Model equation for predicting the tensile strength of resistance-brazed joints. Weld. J. 79, 261–265.

Wang, J., Kusumoto, K., Nezu, K., 2003. Microweld penetration monitoring techniques by arc sensing. In: Proceedings of International Conference on Advanced Intelligent Mechatronics IEEE/ASME, vol. 2, pp. 1027–1030.